Inorganic Chemistry

Article

pubs.acs.org/IC

Role of the Electronically Excited-State Hydrogen Bonding and Water Clusters in the Luminescent Metal−Organic Framework

Xiao Sui, Min Ji, Xin Lan, Weihong Mi, Ce Hao,* and Jieshan Qiu*

State Key Laboratory of Fine Chemicals, Dalian University of Technology, Dalian 116024, Liaoning, China

ABSTRACT: The electronically excited state and luminescence property of metal−organic framework Zn(3-tzba)(2,2′-bipy)(H_2O)·nH_2O have been investigated using the density functional theory (DFT) and time-dependent DFT (TDDFT). The calculated geometry and infrared spectra in the ground state are consistent with the experimental results. The frontier molecular orbitals and electronic configuration indicated that the origin of luminescence is attributed to a ligand-to-ligand charge transfer (LLCT). We theoretically demonstrated that the hydrogen bond H47···O5═C is weakened in the excited state S_1; the weakening of the excited-state hydrogen bonding should be beneficial to the luminescence. To explore the effect of the water clusters on the luminescence, we studied four complexes Zn(3-tzba)(2,2′-bipy)(H_2O)·3H_2O, Zn(3-tzba)(2,2′-bipy)-(H_2O)·2H_2O, Zn(3-tzba)(2,2′-bipy)(H_2O)·H_2O, and Zn(3-tzba)(2,2′-bipy)-(H_2O). The results reveal that the presence of water should play an important role in the emission characteristics of the MOF. Also, the UV−vis absorption and emission spectra of Zn(3-tzba)(2,2′-bipy)(H_2O)·3H_2O are in good agreement with the experimental results.

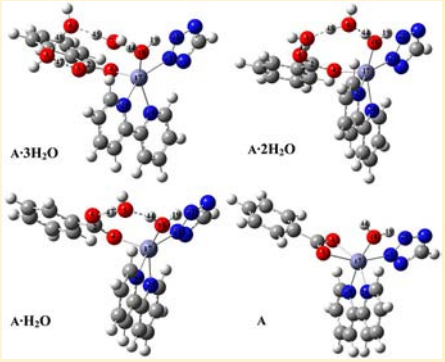

INTRODUCTION

Metal−organic frameworks (MOFs) are extended crystalline materials wherein metal cations are connected by organic linkers.[1] MOFs have made remarkable progress recently because of their fascinating structural diversities and solvent-dependent properties.[2] Due to their diverse properties and highly tunable construction, MOFs have potential applications in the areas of gas storage, molecule recognition, and catalysis.[3−6] This new type of organic−inorganic hybrid material is certainly a very prospective multifunctional luminescent material, because both the inorganic and organic moieties can provide the platforms to generate luminescence. Furthermore, some guest molecules within MOFs can also induce luminescence. On the basis of the ISI Web of Science (retrieved March, 2011), about 10% of 12 717 reported MOFs are luminescent.[7] Currently, luminescent MOFs have great potential applications in luminescent materials, sensors, and photocatalysts.[8−10]

Chen et al.[11] synthesized four new Zn^{II}/Cd^{II} coordination polymers through hydrothermal reaction. Among them, Zn(3-tzba)(2,2′-bipy)(H_2O)·nH_2O (3-H_2tzba =3-(5H-tetrazolyl)-benzoic acid) has a one-dimensional (1D) zigzag chain; the Zn center is surrounded by one 2,2′-bipy molecule, one coordinated water molecule, and two symmetry-related 3-tzba^{2-} (3-(5H-tetrazolyl)benzoate) anions, displaying a distorted octahedral ZnN_3O_3 coordination environment. This blue luminescence of the complex is solvent-dependent. There exists abundant hydrogen bonding within the MOFs. Hydrogen bonding is of vital importance in the construction and luminescent properties of MOFs; therefore, it has been investigated in the design of the functional MOFs.[12−19]

Until now, time-resolved ultrafast spectroscopy, quantum chemical calculations for excited states, and excited-state dynamics simulations have been versatile tools in studying electronic excited-state ultrafast dynamics of complex molecular systems.[20,21] However, ultrafast spectroscopy cannot be used in isolation because of the limited spectral resolution for the femtosecond laser pulses.[22−25] Fortunately, density functional theory (DFT) and time-dependent DFT (TDDFT) provide an effective way to theoretically study the hydrogen bonding in different electronic states.[26] In this study, we employed DFT and TDDFT to investigate excited-state properties of Zn(3-tzba)(2,2′-bipy)(H_2O)·nH_2O. We can confirm the luminescent mechanism based on analysis of the frontier molecular orbitals (MOs) and electronic configuration. Also, we demonstrated the behavior of the hydrogen bonding by comparing the geometric configuration, infrared (IR) spectra, and ^{1}H NMR in the ground state and electronically excited state. The behavior of the coordination bonding was also explored by studying the bond length, bond order, and infrared spectra in the ground and excited state. And then, we studied the influence of these changes on the luminescent properties of Zn(3-tzba)(2,2′-bipy)(H_2O)·nH_2O; thereby we demonstrated the important role of water clusters to the luminescent properties.

COMPUTATIONAL METHODS

The asymmetric unit of Zn(3-tzba)(2,2′-bipy)(H_2O)·nH_2O contains one [Zn(3-tzba)(2,2′-bipy)(H_2O)] motif and three lattice water molecules. We break the 3-tzba, thereby truncating the periodic crystal structure into a representative segment Zn(benzoic acid)(tetrazolyl

Received: November 10, 2012
Published: May 3, 2013

   dx.doi.org/10.1021/ic400924n | *Inorg. Chem.* 2013, 52, 5742−5748

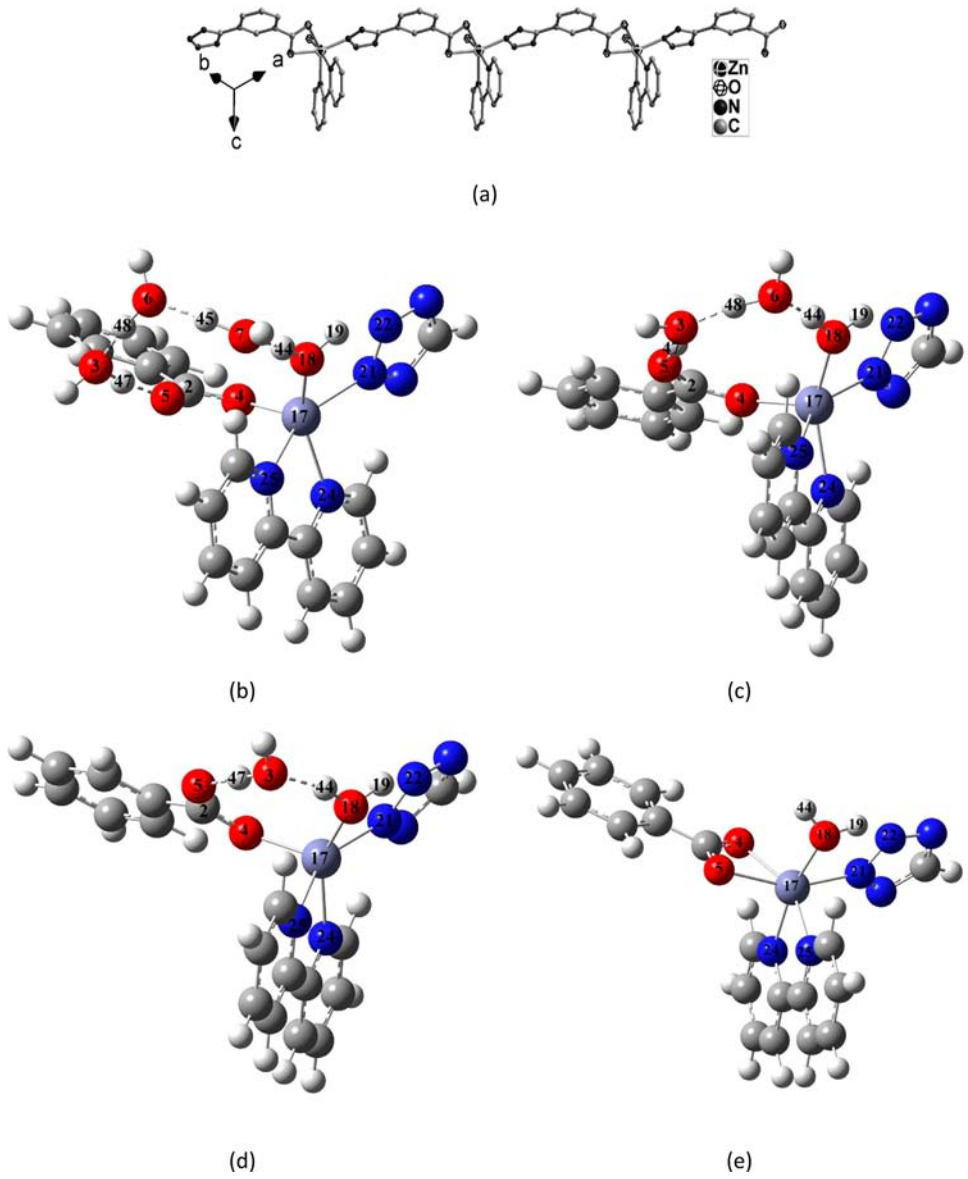

Figure 1. (a) Zigzag chain structure of Zn(3-tzba)(2,2′-bipy)(H_2O); (b) the structure of the representative fragment **A·3H_2O**; (c) the structure of **A·2H_2O**; (d) the structure of **A·H_2O**; (e) the structure of **A**.

ring)(2,2′-bipy)(H_2O)·3H_2O (**A·3H_2O** for short), consisting of one benzoic acid, one tetrazolyl ring, and three water molecules (Figure 1b). Meanwhile, some important atoms are labeled in the figure. The ground-state geometric optimization was performed by using the DFT method with the hybrid exchange-correlation functional of the Coulomb-attenuating method (CAM-B3LYP) functional using the Gaussian 09 program suite,[27−30] when the excited-state electronic structures were calculated using the TDDFT method with the same CAM-B3LYP functional. The relativistic effects are taken into account by using the (LANL2DZ) basis sets in both the ground-state and excited-state geometric optimizations. The ground-state and excited-state IR spectra were calculated and scaled using the optimized ground-state and excited-state structures, respectively, and the scaling factor is 0.961 (NIST Computational Chemistry Comparison and Benchmark Database NIST Standard Reference Database Number 101 Release 15b, August 2011, Editor: Russell D. Johnson III http://cccbdb.nist.gov/). For NMR, we used the LANL2DZ basis sets for Zn atom and the 6-311G++(d, p) basis sets for other atoms, respectively. For energies, we used the LANL2DZ basis sets for Zn atom and the 6-311G+(d) basis sets for other atoms, respectively. Long-range-corrected (LC) DFT/TDDFT methods provide an accurate description of charge-transfer excitations.[31−33] It is very important to note that the original CAM-B3LYP functional which exhibits a −0.65/r dependence is not sufficient. The CAM-B3LYP functional is particularly different than the other LC functionals since it does not incorporate a full 100% Hartree−Fock (HF) exchange, which is essential for accurately describing the HOMO→LUMO transition.[34] Therefore, we also performed the calculation of the excitation energy with the LC-BLYP functional. In the case of the CAM-B3LYP functional, the UV−vis spectrum shows the excitation energy is 271 nm, while the energy is 261 nm with the LC-BLYP functional. Moreover, with the CAM-B3LYP functional the calculated absorption peak at 271 nm is more consistent with experimental results at 274 nm. Thus, using the CAM-B3LYP functional to calculate excitation energy is appropriate in our system. In addition, we compared the difference between the experimental and calculated spectra of the ligand, and thereby scaled the electronic spectra according to the difference.

RESULTS AND DISCUSSION

Ground-State Geometric Optimization. The crystalline structure of Zn(3-tzba)(2,2′-bipy)(H_2O)·$n$$H_2O$ has a 1D zigzag chain.[11] Figure 1a shows the zigzag chain structure of Zn(3-

dx.doi.org/10.1021/ic400924n | Inorg. Chem. 2013, 52, 5742−5748

tzba)(2,2′-bipy)(H_2O)·nH_2O. To avoid the complexity of periodic structures, the Zn-based complexes are truncated into representative fragment Zn(benzoic acid)(tetrazolyl ring)-(2,2′-bipy)(H_2O)·3H_2O (**A·3H_2O**) from crystal structure for theoretical computation. In addition, we also changed the amount of lattice water molecules within the hydrogen bonded **A·3H_2O** for study: Zn(benzoic acid)(tetrazolyl ring)(2,2′-bipy)(H_2O)·2H_2O (**A·2H_2O**), Zn(benzoic acid)(tetrazolyl ring)(2,2′-bipy)(H_2O)·H_2O (**A·H_2O**), and Zn(benzoic acid)-(tetrazolyl ring)(2,2′-bipy)(H_2O) (**A**) as shown in Figure 1. It is noted that different number of intermolecular hydrogen bonds are formed in **A·3H_2O**, **A·2H_2O**, and **A·H_2O**.

The geometric optimization of the representative fragment **A·3H_2O** in the ground state is carried out using the DFT method with the CAM-B3LYP functional (Figure 1b). We also calculated the vibrational frequency of **A·3H_2O** in the ground state using the DFT method with the CAM-B3LYP functional. Moreover, we optimize the ground-state geometric conformations with the LC-BLYP functional. Comparisons of the calculated bond lengths, dihedral angles, and IR spectral values with reported values are listed in Table 1 and Figure 2,

Table 1. Calculated and Experimental Values of Zn(3-tzba)(2,2′-bipy)(H_2O)·3H_2O (A·3H_2O)

	calcd value (CAM-B3LYP)/(LC-BLYP)	exptl value[a]
	Bond Lengths (Å)	
Zn17−O4	1.99/1.98	2.22
Zn17−O18	2.02/2.01	2.09
Zn17−N21	2.12/2.09	2.05
Zn17−N24	2.19/2.15	2.16
N21−N22	1.36/1.35	1.32
C2−O4	1.29/1.30	1.27
O18−H44···O6	1.52/1.49	1.98
	Bond Angles (deg)	
N21−Zn17−O18	83.06/83.21	91.15
N21−Zn17−O4	105.63/105.46	104.16
O18−Zn17−O4	111.83/109.84	98.57
O5−Zn17−O18	85.76/85.27	87.02
N24−Zn17−N25	75.19/76.14	76.56
O4−Zn17−N24	98.50/98.45	88.97
O18−Zn17−N25	92.87/93.38	93.09
N21−Zn17−N24	93.56/93.64	94.44

[a]Reference 11.

respectively. Figure 2 clearly shows that our simulated spectra are in good agreement with the real data in terms of frequencies from 2000 to 400 cm^{-1}, i.e., COO asymmetrical and symmetrical stretching bands. From Table 1, we can find that the calculated bond lengths and angles agree well with the experimental data, except the lengths of hydrogen bond O18−H44···O6. It is because X-ray diffraction cannot obtain the position of hydrogen atom accurately without being combined with neutron diffraction. After the comparison, values of the calculated bond lengths and dihedral angles with the CAM-B3LYP functional are consistent with that with the LC-BLYP functional. The accuracy of computed results in bond length is within experimental errors 0.1 Å, but the dihedral angle between the carboxylate group and the benzene is about 5° which is different from 31° in the real MOF. Although the structure changes during optimization, the calculated electronic spectra and IR show that the representative fragment **A·3H_2O** as a calculated model is reasonable.

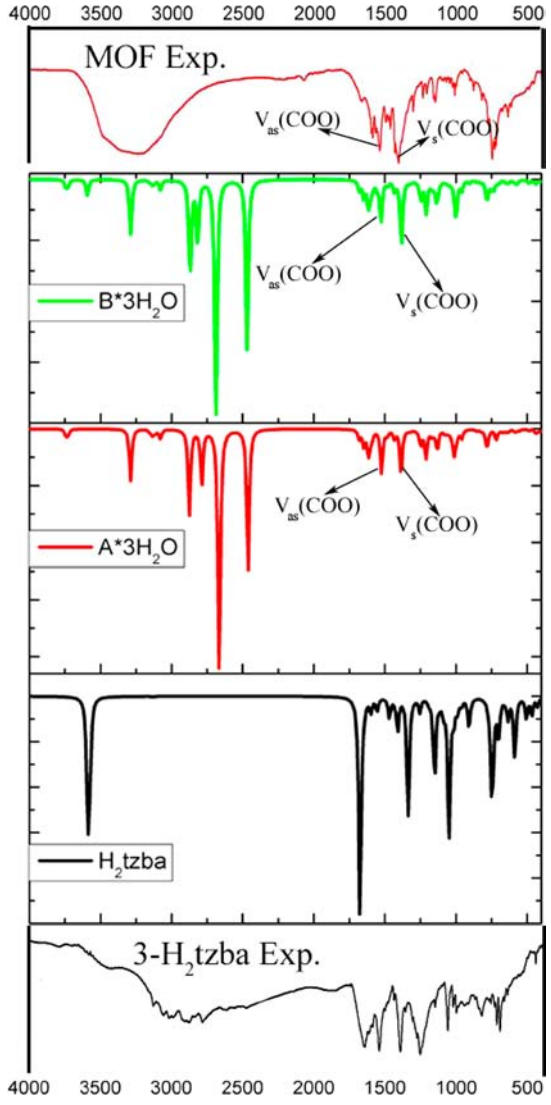

Figure 2. Comparison of the simulated IR spectra and experimental data (ref 11) in the ground state.

Frontier Molecular Orbitals and Electronic Configuration. Molecular orbital (MO) analysis can provide insight into the nature of the excited states directly. On the basis of Kasha's rule, in principle, photon emission (fluorescence or phosphorescence) occurs in appreciable yields only from the lowest excited state of a given multiplicity (S_1 and T_1).[35] Herein we mainly discuss the S_1 state of **A·3H_2O**. The frontier molecular orbitals and the electronic configuration of **A·3H_2O** are presented in Figure 3a. From the frontier molecular orbitals, we can find that the electron density distribution of LUMO orbital is localized in the 2,2′-bipy ligand, when that of HOMO orbital is localized in the benzoic acid ligand. A further observation indicates that the HOMO and LUMO orbitals have π and π^* character, respectively. Thus, it is evident that the S_1 state has $\pi-\pi^*$ character. From the electronic configuration, the majority of electrons of the C and N atoms of the 2,2′-bipy ligand contribute to LUMO, while HOMO is attributed to the electrons on the C and O atoms of the benzoic acid ligand. Therefore, by the analysis of the frontier molecular orbitals and electronic configuration, we can conclude that the emission is attributed to a ligand-to-ligand charge transfer (LLCT). Moreover, we also truncate and optimize the ground-state

dx.doi.org/10.1021/ic400924n | Inorg. Chem. 2013, 52, 5742−5748

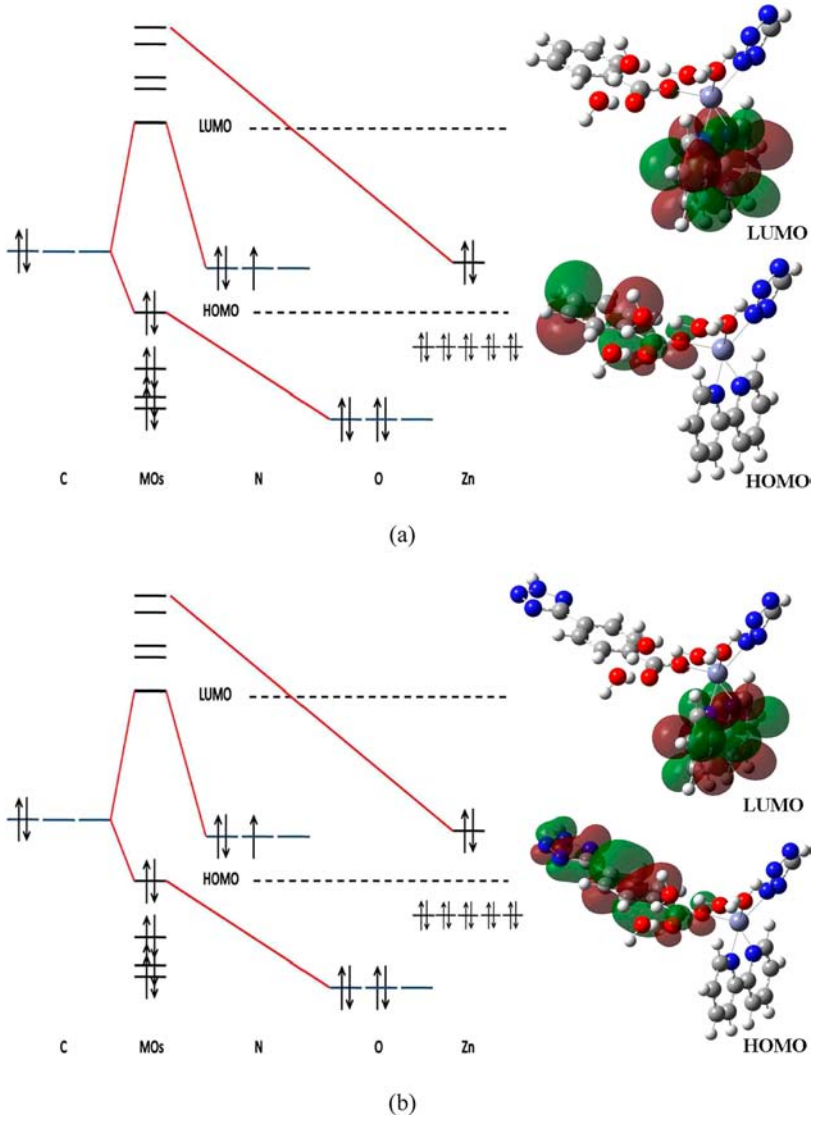

Figure 3. (a) Calculated frontier molecular orbitals (MOs) of **A·3H$_2$O** and its corresponding electronic configurations. (b) Calculated frontier molecular orbitals (MOs) of **B·3H$_2$O** and its corresponding electronic configurations.

geometric conformations of Zn(tetrazolyl ring)(3-tzba)(2,2′-bipy)(H_2O)·3H_2O (**B·3H$_2$O** for short). Then, we calculated the energy of **B·3H$_2$O**. From the analysis of the frontier molecular orbitals and electronic configuration (Figure 3b), we can find that the electron density distribution of LUMO and HOMO orbital of **A·3H$_2$O** are almost the same with that of **B·3H$_2$O.** Also, we can also find that there is no difference between **A·3H$_2$O** and **B·3H$_2$O** in emission origin (LLCT). Therefore, it is reasonable and reliable to use the representative fragment **A·3H$_2$O** as a calculated model.

Behavior of Hydrogen Bonding in the Electronically Excited State. On the basis of the analysis of the frontier molecular orbitals and the electronic configuration, it is inferred that only the H47···O5═C2 could be related with luminescent property of the MOF. In order to investigate in detail the behavior of the hydrogen bonding in the electronically excited state, we systematically calculated and discussed the lengths related to the intermolecular hydrogen bond H47···O5═C2. However, experimental NMR shifts and IR spectra are much more sensitive and detective than geometry; therefore, we calculated ^{1}H NMR and vibrational spectra in S_0, S_1. Table 2 shows the calculated lengths and ^{1}H NMR chemical shifts of the hydrogen bond H47···O5═C2 in the ground and excited states.

Table 2. Calculated Bond Length of H47···O5═C2 and ^{1}H NMR of H47 for Zn(3-tzba)(2,2′-bipy)(H_2O)·3H_2O (A·3H_2O)

H47···O5═C2	S_0	S_1
bond length (Å)	1.47	1.49
^{1}H NMR of H47 (ppm)	17.9	18.8

It is obvious that the length of hydrogen bond H47···O5═C2 is slightly increased from 1.47 Å in the S_0 state to 1.49 Å in the S_1 state. The hydrogen bond length is elongated by 0.02 Å from the S_0 to S_1 state. It reveals that the intermolecular hydrogen bond H47···O5═C2 could be weakened upon excitation to the S_1 state.

^{1}H NMR spectra can show that the appropriate charge redistribution takes place within the deprotonated species.[36] The weakening of the hydrogen bonding increases the distance

dx.doi.org/10.1021/ic400924n | Inorg. Chem. 2013, 52, 5742−5748

between its proton-acceptor and H atom. Also, the electron density of the hydrogen nucleus reduces. Therefore, the deshielding effect enhances, and the ^{1}H NMR chemical shift increases, and vice versa. As shown in Table 2, the signal at δ = 18.8 ppm is assigned to the proton of H_{47} in the S_1 state, which is shifted downfield when compared to that in the S_0 state (δ = 17.9 ppm). It can demonstrate that the hydrogen bonding is weakened in the excited state.

It has been demonstrated that the excited-state hydrogen-bonding behavior can be investigated by monitoring the characteristic vibrational modes involved in the hydrogen bond formation.[37] According to the method, the excited-state hydrogen bond could be strengthened if the infrared spectra of groups forming hydrogen bonding show the red shift from the ground to excited state. Otherwise, the blue shift means the weakening of hydrogen bonding. Figure 4 shows the calculated

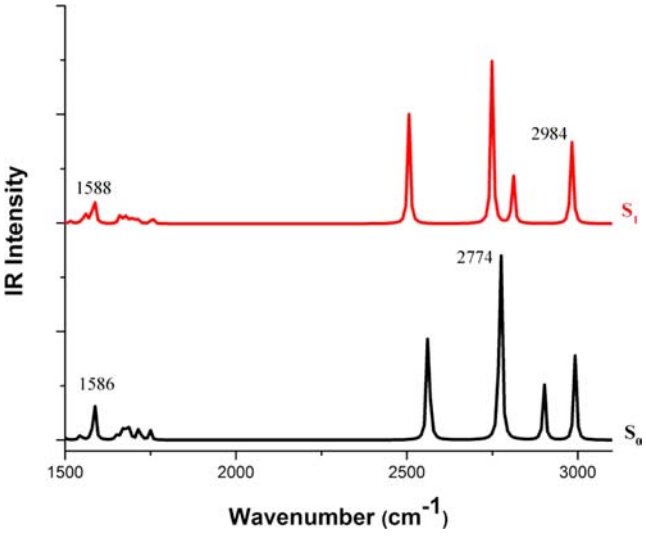

Figure 4. Calculated IR spectra of **A·3H$_2$O** in the ground and excited state.

IR spectral shifts of the characteristic vibrational modes involved in the formation of hydrogen bonds in the S_0, S_1 states. It shows that the stretching of C2═O5 group is blue-shifted from 1586 cm^{-1} in the S_0 state to 1588 cm^{-1} in the S_1 state. Meanwhile, the stretching of O3−H47 group also blue shifts by 210 cm^{-1} from the S_0 state to the S_1 state. A blue shift of the C2═O5 and O3−H47 stretching mode can demonstrate that the hydrogen bond H47···O5═C2 is significantly weakened.

From the length of hydrogen bond, ^{1}H NMR, and IR spectra, we conclude that the hydrogen bond H47···O5═C2 is weakened in the S_1 state. The weakening of the hydrogen bond in the S_1 state decreases the attraction on the electrons of O5 atom, and goes against the charge transfer from 2,2′-bipy ligand to benzoic acid ligand. Thus, it can be inferred that the weakening of the hydrogen bond in the S_1 state should be beneficial to the luminescence.

Effect of Water Clusters on the Luminescent Properties. Water is of fundamental importance for human life and plays an important role in many biological and chemical systems. In chemistry, a water cluster is a discrete hydrogen bonded assembly or cluster of water molecules,[38] and could influence the optical properties of luminescent material by causing the structure changes. In our work, we calculated and compared the properties of four complexes Zn(benzoic acid)(tetrazolyl ring)(2,2′-bipy)(H_2O) (**A**), Zn(benzoic acid)-(tetrazolyl ring)(2,2′-bipy)(H_2O)·H_2O (**A·H$_2$O**), Zn(benzoic acid)(tetrazolyl ring)(2,2′-bipy)(H_2O)·2H_2O (**A·2H$_2$O**), and Zn(benzoic acid)(tetrazolyl ring)(2,2′-bipy)(H_2O)·3H_2O (**A·3H$_2$O**) in order to understand the role of water clusters in luminescent properties.

From the frontier molecular orbitals and electronic configuration, we can speculate that only the three coordination bonds Zn17−O4, Zn17−N24, and Zn17−N25 could be related to luminescence. As shown in Table 3, the bond length of Zn17−O4 of the representative fragment **A** is increased from the S_0 to S_1 state, when that of Zn17−N24 and Zn17−N25 is shortened. It is indicated that Zn17−O4 is weakened, and Zn17−N24 and Zn17−N25 become strengthened in the S_1 state. However, for the hydrogen-bonded complex **A·H$_2$O** from the S_0 to S_1 state, the coordination bond Zn17−O4 is shortened by 0.03 Å, when the bond length of Zn17−N24 is increased by 0.54 Å and that of Zn17−N25 is shortened by 0.12 Å. For the complex **A·2H$_2$O**, from the S_0 to S_1 state, the bond length of Zn17−O4 is also shortened by 0.03 Å, while that of Zn17−N24 is increased by 0.55 Å and that of Zn17−N25 is shortened by 0.11 Å. Also, for the complex **A·3H$_2$O**, the bond length of Zn17−O4 is shortened by 0.01 Å from the S_0 to S_1 state, while that of Zn17−N24 is increased by 0.58 Å and that of Zn17−N25 is shortened by 0.09 Å. It indicated that, for the complexes **A·H$_2$O**, **A·2H$_2$O**, and **A·3H$_2$O**, the Zn17−O4 is strengthened, while Zn17−N24 is weakened in the excited state.

Figure 5 shows the infrared spectra of **A**, **A·H$_2$O**, **A·2H$_2$O**, and **A·3H$_2$O** in the S_0 and S_1 state. In Figure 5, it is clearly shown that, in the complex **A**, the vibrational stretching mode frequency for the Zn17−O4 bond is red-shifted by 60 cm^{-1} from 436 cm^{-1} in the S_0 state to 376 cm^{-1} in the S_1 state. Meanwhile, the stretching frequencies for the Zn17−N24 and Zn17−N25 bonds are blue-shifted from the S_0 to S_1 state. In the complex **A·H$_2$O**, the stretching frequency for the Zn17−O4 bond is almost unchanged in the S_1 state, while that of **A·2H$_2$O** is blue-shifted by 14 cm^{-1} from the S_0 to S_1 state. Also, the stretching frequency for the Zn17−O4 bond of **A·3H$_2$O** is blue-shifted by 12 cm^{-1} from the S_0 to S_1 state. Moreover, in the **A·H$_2$O**, **A·2H$_2$O**, and **A·3H$_2$O** the stretching frequencies for the Zn17−N24 and Zn17−N25 bonds are red-shifted in S_1 state. The results shows that, in the **A**, the coordination bond Zn17−O4 is weakened, when the Zn17−N24 and Zn17−N25

Table 3. Bond Lengths of the Coordination Bonds of A, A·H$_2$O, A·2H$_2$O, and A·3H$_2$O in the S_0 and S_1 State

	A		**A·H$_2$O**		**A·2H$_2$O**		**A·3H$_2$O**	
bond length (Å)	S_0	S_1	S_0	S_1	S_0	S_1	S_0	S_1
Zn17−O4	2.18	2.23	1.98	1.95	1.97	1.94	1.99	1.98
Zn17−N24	2.16	2.06	2.17	2.71	2.19	2.74	2.19	2.77
Zn17−N25	2.16	2.04	2.18	2.06	2.18	2.07	2.17	2.08

dx.doi.org/10.1021/ic400924n | Inorg. Chem. 2013, 52, 5742−5748

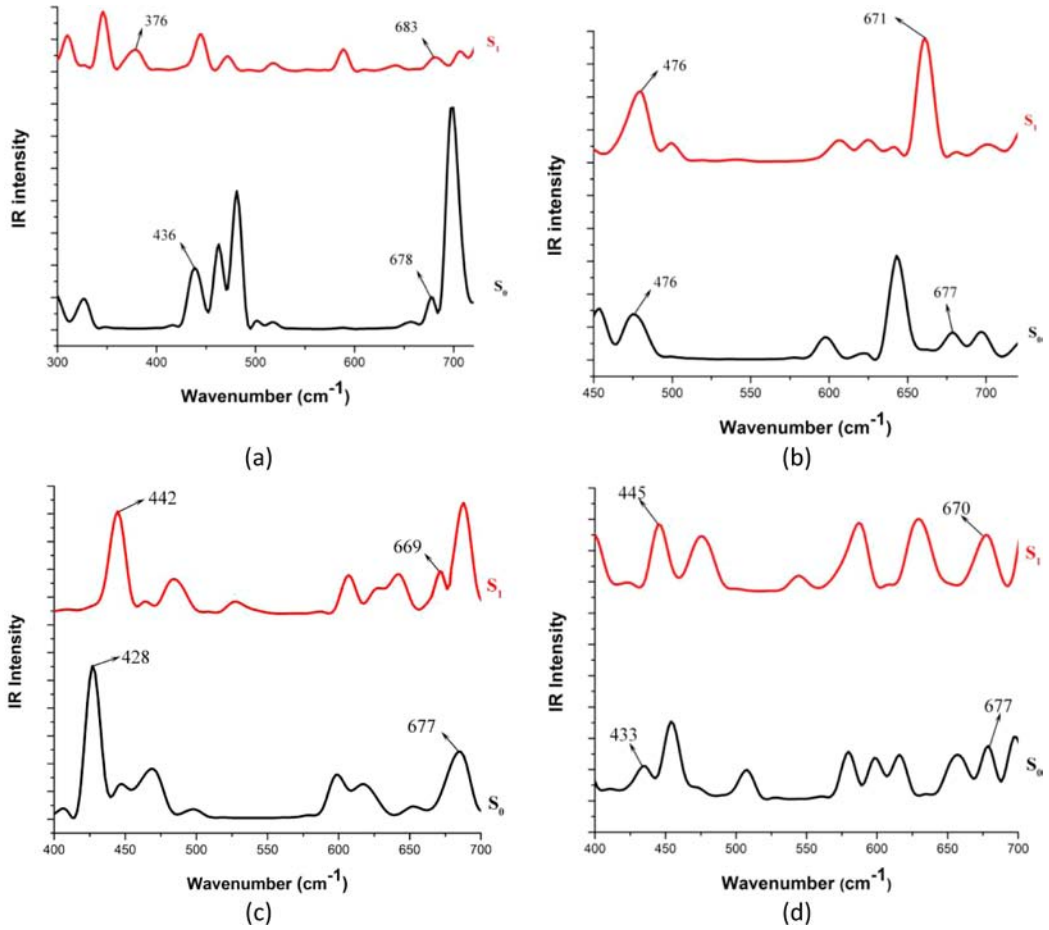

Figure 5. (a) Calculated stretching frequencies for the Zn17−O4, Zn17−N24, and Zn17−N25 bonds of **A**. (b) The stretching frequencies for the Zn17−O4, Zn17−N24, and Zn17−N25 bonds of **A·H$_2$O**. (c) The stretching frequencies for the Zn17−O4, Zn17−N24, and Zn17−N25 bonds of **A·2H$_2$O**. (d) The stretching frequencies for the Zn17−O4, Zn17−N24, and Zn17−N25 bonds of **A·3H$_2$O**.

Table 4. Comparison of the Calculated Emission Spectra between A, A·H$_2$O, A·2H$_2$O, and A·3H$_2$O[a]

	A fluor	**A·H$_2$O** fluor	**A·2H$_2$O** fluor	**A·3H$_2$O** abs	fluor	
scaled calcd (nm/eV)	449/2.76	446/2.78	445/2.79	271/4.58	399/3.11	472/2.63
exptl[b] (nm)				274	437	470

[a]The calculated absorption spectrum of **A·3H$_2$O** and the experimental values of the MOF are also listed. [b]Reference 11.

bonds tend to be strengthened in the S_1 state. However, the Zn17−O4 bond is strengthened, while the Zn17−N24 and Zn17−N25 bonds are weakened in the S_1 state of both **A·H$_2$O**, **A·2H$_2$O**, and **A·3H$_2$O**. The results are consistent with the changes in bond lengths.

For the **A**, due to the weakening of the coordination bond Zn17−O4 and the strengthening of Zn17−N24, Zn17−N25, it favors the charge transfer from the ligand to the ligand, and goes against the luminescence. However, in the complex **A·H$_2$O**, **A·2H$_2$O**, and **A·3H$_2$O**, the strengthening of Zn17−O4 and the weakening of Zn17−N24 should be in favor of luminescence because it goes against the charge transfer form ligand to ligand. Moreover, it can be inferred from the comparison in detail that the fluorescent intensity of the three hydrogen complexes could change in the following order: **A** < **A·3H$_2$O** ≤ **A·H$_2$O** < **A·2H$_2$O**.

As listed in Table 4, we also calculated the emission spectra of **A**, **A·H$_2$O**, **A·2H$_2$O**, and **A·3H$_2$O**. One can be found that, from **A** to **A·2H$_2$O**, the energy gap between the excited state and ground state will decrease as amounts of water molecules within the system increase. Therefore, it can be inferred that from **A** to **A·2H$_2$O** the rate of radiation transition from the excited to the ground state is enhanced, while the rate of internal conversion (IC) is weakened according to the transition rate equations.[39−41] The change of transition rate is consistent with the above variation of fluorescent intensity. In addition, the calculated UV−vis absorption and emission spectra of **A·3H$_2$O** are also presented. After scaling the electron spectra, the calculated absorption peak at 271 nm is in good agreement with experimental results at 274 nm. Also, the two emission peaks at 399 nm and 472 nm conform well to the experimental peak at 437 and 470 nm.

■ CONCLUSIONS

Through the detailed investigation of the representative fragment of the solvent-dependent luminescent MOF Zn(3-tzba)(2,2′-bipy)(H_2O)·$n$$H_2O$, we made the following important conclusions: (1) The calculated results for geometric, vibrational, and electronic structure are in good agreement with the experimental results. It has shown that the truncated

dx.doi.org/10.1021/ic400924n | Inorg. Chem. 2013, 52, 5742−5748

representative fragments we used in this investigation are reasonable and reliable. (2) The calculated frontier molecular orbitals and electronic configuration of the hydrogen-bonded complex **A·3H$_2$O** indicated that the luminescence should be the ligand-to-ligand charge transfer form. (3) The comparison of the geometry, ^{1}H NMR, and vibrational spectra in the ground and electronically excited states indicated that the intermolecular hydrogen bond H47···O5═C2 related with the luminescence is weakened in the excited state. Also, we have demonstrated that the hydrogen bond weakening is beneficial to luminescence of the MOF. (4) Through calculating the bond lengths and vibrational frequencies of the coordination bonds of the three complexes **A**, **A·H$_2$O**, **A·2H$_2$O**, and **A·3H$_2$O** and comparing their energy gap between the excited state and ground state, we explored the influence of the water clusters on the luminescence of the MOF. It can be inferred that the increase of appropriate amounts of water molecules within the MOF should be in favor of the luminescence. (5) These findings can clarify that the luminescent properties of MOFs could be controlled by adjusting the behaviors of the hydrogen bonding and water clusters; this provides an effective guidance to design and synthesize functional MOFs of higher luminescence efficiency.

AUTHOR INFORMATION

Corresponding Author

*E-mail: haoce@dlut.edu.cn. Phone: +86-411-84986335. Fax: +86-411-84748086 (C.H); E-mail: jqiu@dlut.edu.cn. Phone: +86-411-84986024. Fax: +86-411-84986024 (J.Q.).

Notes

The authors declare no competing financial interest.

ACKNOWLEDGMENTS

Support of this work by the National Natural Science Foundation of China (Grants 21036006, 21137001) and the Dalian Scientific Program (No. 2011A15GX023) is gratefully acknowledged.

REFERENCES

(1) Kreno, L. E.; Leong, K.; Farha, O. K.; Allendorf, M.; Van Duyne, R. P.; Hupp, J. T. *Chem. Rev.* **2012**, *112*, 1105−1125.
(2) Lin, J. G.; Qiu, L.; Wang, F. M.; Lu, C. S.; Meng, Q. J.; Wu, P. H. *Inorg. Chem. Commun.* **2010**, *13*, 175−178.
(3) Yu, J. H.; Zhu, Y. C.; Wu, D.; Yu, Y.; Hou, Q.; Xu, J. Q. *J. Chem. Soc., Dalton Trans.* **2009**, *39*, 8248−8256.
(4) Getman, R. B.; Bae, Y. S.; Wilmer, C. E.; Snurr, R. Q. *Chem. Rev.* **2012**, *112*, 703−723.
(5) Horcajada, P.; Gref, R.; Baati, T.; Allan, P. K.; Guillaume Maurin, G.; Couvreur, P.; Ferey, G.; Morris, R. E.; Serre, C. *Chem. Rev.* **2012**, *112*, 1232−1268.
(6) Li, J. R.; Sculley, J.; Zhou, H. C. *Chem. Rev.* **2012**, *112*, 869−932.
(7) Betard, A.; Fischer, R. A. *Chem. Rev.* **2012**, *112*, 1055−1083.
(8) Xu, H.; Huanga, L. F.; Guo, L. M.; Zhang, Y. G.; Rena, X. M.; Song, Y.; Xie, J. *J. Lumin.* **2008**, *128*, 1665−1672.
(9) Stock, N.; Biswas, S. *Chem. Rev.* **2012**, *112*, 933−969.
(10) Liu, Y. H.; Zhao, G. J.; Li, G. Y.; Han, K. L. *J. Photochem. Photobiol., A* **2010**, *209*, 181−185.
(11) Chen, F.; Wu, M. F.; Liu, G. N.; Wang, M. S.; Zheng, F. K.; Yang, C.; Xu, Z. N.; Liu, Z. F.; Guo, G. C.; Huang, J. S. *Eur. J. Inorg. Chem.* **2010**, *31*, 4982−4991.
(12) Beatty, A. M. *Cryst. Eng. Commun.* **2001**, *51*, 1−13.
(13) Domcke, W.; Sobolewski, A. L. *Science* **2003**, *302*, 1693−1694.
(14) Zhao, G. J.; Han, K. L. *J. Phys. Chem. A* **2009**, *113*, 14329−14335.
(15) Zhao, G. J.; Han, K. L. *Phys. Chem. Chem. Phys.* **2010**, *12*, 8914−8918.
(16) Zhao, G. J.; Liu, J. Y.; Zhou, L. C.; Han, K. L. *J. Phys. Chem. B* **2007**, *111*, 8940−8945.
(17) Samant, V.; Singh, A. K.; Ramakrishna, G.; Ghosh, H. N.; Ghanty, T. K.; Palit, D. K. *J. Phys. Chem. A* **2005**, *109*, 8693−8704.
(18) Jin, L.; Zhai, J.; Heng, L.; Wei, T.; Wen, L.; Jiang, L.; Zhao, X.; Zhang, X. *J. Photochem. Photobiol., C* **2009**, *10*, 149−158.
(19) Han, J.; Meng, J. B. *J. Photochem. Photobiol., C* **2009**, *10*, 141−147.
(20) Gehlen, M. H.; De Schryver, F. C. *Chem. Rev.* **1993**, *97*, 11242−11248.
(21) Zhao, G. J.; Han, K. L.; Lei, Y. B.; Dou, Y. *J. Chem. Phys.* **2007**, *127*, 094307−1−6.
(22) Chen, R. K.; Zhao, G. J.; Yang, X. C.; Jiang, X.; Liu, J. F.; Tian, H. N.; Gao, Y.; Han, K. L.; Sun, M. T.; Sun, L. C. *J. Mol. Struct.* **2008**, *876*, 102−109.
(23) Harju, T. O.; Huizer, A. H.; Varma, C. *Chem. Phys.* **1995**, *200*, 215−224.
(24) Kim, T. G.; Wolford, M. F.; Topp, M. R. *Photochem. Photobiol. Sci.* **2003**, *2*, 576−584.
(25) Das, S.; Datta, A.; Bhattacharyya, K. *J. Phys. Chem. A* **1997**, *101*, 3299−3304.
(26) Wu, D. Y.; Mi, W. H.; Ji, M.; Hao, C.; Qiu, J. S. *Spectrochim. Acta, Part A* **2012**, *97*, 589−593.
(27) Becke, A. D. *J. Chem. Phys.* **1993**, *98*, 5648−5652.
(28) Perdew, J. P. *Phys. Rev. B* **1986**, *33*, 8822−8824.
(29) Yanai, T.; Tew, D. P.; Handy, N. C. *Chem. Phys. Lett.* **2004**, *393*, 51−57.
(30) Frisch, M. J.; Trucks, G. W.; Schlegel, H. B.; Scuseria, G. E.; Robb, M. A.; Cheeseman, J. R.; Scalmani, G.; Barone, V.; Mennucci, B.; Petersson, G. A.; Nakatsuji, H.; Caricato, M.; Li, X.; Hratchian, H. P.; Izmaylov, A. F.; Bloino, J.; Zheng, G.; Sonnenberg, J. L.; Hada, M.; Ehara, M.; Toyota, K.; Fukuda, R.; Hasegawa, J.; Ishida, M.; Nakajima, T.; Honda, Y.; Kitao, O.; Nakai, H.; Vreven, T.; Montgomery, J. A., Jr.; Peralta, J. E.; Ogliaro, F.; Bearpark, M.; Heyd, J. J.; Brothers, E.; Kudin, K. N.; Staroverov, V. N.; Kobayashi, R.; Normand, J.; Raghavachari, K.; Rendell, A.; Burant, J. C.; Iyengar, S. S.; Tomasi, J.; Cossi, M.; Rega, N.; Millam, J. M.; Klene, M.; Knox, J. E.; Cross, J. B.; Bakken, V.; Adamo, C.; Jaramillo, J.; Gomperts, R.; Stratmann, R. E.; Yazyev, O.; Austin, A. J.; Cammi, R.; Pomelli, C.; Ochterski, J. W.; Martin, R. L.; Morokuma, K.; Zakrzewski, V. G.; Voth, G. A.; Salvador, P.; Dannenberg, J. J.; Dapprich, S.; Daniels, A. D.; Farkas, O.; Foresman, J. B.; Ortiz, J. V.; Cioslowskiand, J.; Fox. D. J. *Gaussian 09, Revision A.02*; Gaussian, Inc.: Wallingford CT, 2009.
(31) Wong, B. M.; Piacenza, M. F.; Sala, D. *Phys. Chem. Chem. Phys.* **2009**, *11*, 4498−4508.
(32) Kityk, A. V. *J. Phys. Chem. A* **2012**, *116*, 3048−3055.
(33) Balanay, M. P.; Kim, D. H. *J. Phys. Chem.* **2011**, *115*, 19424−19430.
(34) Wong, B. M.; Hsieh, T. H. *J. Chem. Theory Comput.* **2010**, *6*, 3704−3712.
(35) Kasha, M. *Discuss. Faraday Soc.* **1950**, *9*, 14−19.
(36) Li, G. Y.; Zhao, G. J.; Liu, Y. H.; Han, K. L.; He, G. Z. *J. Comput. Chem.* **2010**, *31*, 1759−1765.
(37) Zhao, G. J.; Han, K. L. *J. Phys. Chem. A* **2007**, *111*, 2469−2474.
(38) Ludwig, R. *Angew. Chem., Int. Ed.* **2001**, *40*, 1808−1827.
(39) Zhao, G. J.; Han, K. L. *Acc. Chem. Res.* **2012**, *45*, 404−413.
(40) Peng, Q.; Yi, Y. P.; Shuai, Z. G. *J. Chem. Phys.* **2007**, *126*, 114302−1−8.
(41) Englman, R.; Jortner, J. *Mol. Phys.* **1970**, *18*, 145−164.